Carbohydrate Polymers 90 (2012) 1573–1581

Contents lists available at SciVerse ScienceDirect

Carbohydrate Polymers

journal homepage: www.elsevier.com/locate/carbpol

Biomimetic growth of hydroxyapatite on phosphorylated electrospun cellulose nanofibers

Kaina Li[a], Jiangnan Wang[a], Xinqing Liu[b], Xiaopeng Xiong[c], Haiqing Liu[a,*]

[a] Key Laboratory of Polymer Materials of Fujian Province, College of Materials Science and Engineering, Fujian Normal University, Fujian 350007, China
[b] People's Hospital of Jiangxi Province, Nanchang 330006, China
[c] Department of Materials Science and Engineering, College of Materials, Xiamen University, Xiamen 361005, China

ARTICLE INFO

Article history:
Received 25 April 2012
Received in revised form 19 June 2012
Accepted 9 July 2012
Available online 16 July 2012

Keywords:
Electrospinning
Nanofiber
Hydroxyapatite
Cellulose biocomposite

ABSTRACT

In biomimicking the formation of collagen fiber/hydroxyapatite (HAp) in natural bone, electrospun cellulose nanofiber (CelluNF)/HAp composites were synthesized in simulated body fluid (SBF). Their morphology and structure were characterized by SEM, TEM, XRD and XPS. CelluNFs showed low bioactivity in inducing the growth of HAp. In order to improve this ability, CelluNFs were slightly phosphorylated with a degree of substitution of phosphate group of 0.28. The modified CelluNFs were highly effective in guiding the HAp growth along the fibers. The HAp crystal size in the composites was ca. 24 nm, and the lattice spacing of (2 1 1) plane was 2.83 Å. It was found that the HAps in the composites were calcium deficient. The CelluNF/HAp composites are highly porous materials with micro-, meso-, and macro-pores. A mechanism for the HAp growth on CelluNFs was presented. Such CelluNF/HAp composites can be potentially useful in the field of bone tissue engineering.

1. Introduction

Synthetic bioactive bone grafts materials have been in a high demand because of a shortage of autografts and the immunological rejection reaction of allografts (Juhasz & Best, 2012). In mimicking the collagen fiber/hydroxyapatite (HAp) composite structure of natural bone, several kinds of fibers such as silk fibers, peptide-amphiphile nanofibers, and cellulose nanofibers with biocompatibility have been applied to guide mineralization of HAp to form composite materials. For instance, silk/calcium phosphate scaffolds with mechanical properties comparable to cancellous bone were reported for load-bearing osteregenerative applications (Collins et al., 2009). Crosslinked self-assembled peptide-amphiphile nanofibers directed growth of HAp. In this composite the crystallographic *c* axes of HAp were aligned with the long axes of the fibers, mimicking that observed between collagen fibrils and HAp crystals in natural bone (Hartgerink, Beniash, & Stupp, 2001).

As far as the stability and mechanical properties are concerned, cellulose fiber appears to be a superior choice. Therefore, the fabrication of cellulose/HAp composite scaffolds is intriguing to many researchers in recent years (He, Chang, Peng, & Zhang, 2012; Wan et al., 2009; Zimmermann, LeBlanc, Sheets, Fox, & Gatenholm, 2011). The reasons for the selection of cellulose as supporting scaffolds are: (I) abundance and renewability of this naturally-occurring polymer; (II) stable good mechanical properties in physiological environments in vitro and in vivo aging; (III) negligible foreign body and inflammatory response reactions in vitro and in vivo applications (Backdahl et al., 2006; Klemm, Schumann, Udhardt, & Marsch, 2001; Märtson, Viljanto, Hurme, Laippala, & Saukko, 1999; Rodriguez, Renneckar, & Gatenholm, 2011); (IV) abundant reactive hydroxyl groups on the macromolecular chains; (V) biodegradability by a combination of chemical, biological and mechanical processes. Though cellulose shows poor biodegradation in vivo within a short time period of application such as wound healing, the cellulose material used as a permanent implantable scaffold for tissue engineering is degradable in the long term. For instance, in an in vivo subcutaneous study in the rat, it was found that the cellulose sponge completely disappeared from subcutaneous tissue after 60 weeks (Märtson et al., 1999). The in vivo biodegradability can be effectively improved by increasing the amorphous regions (in other words, lowering the crystallinity) and augmenting the hydrophilicity of cellulose materials (Entcheva et al., 2004; Miyamoto, Takahashi, Ito, Inagaki, & Noishiki, 1989). Additionally, the final product of the cellulose degradation process is glucose—a natural nutrient for the cells, as compared to the acidic byproducts of the biodegradable PLGA scaffolds.

Among the many types of cellulose fibers, bacterial cellulose (BC) fibers have been particularly studied for applications of fiber reinforced HAp composites, due largely to their nanometer size

* Corresponding author. Tel.: +86 591 83404938; fax: +86 591 83404938.
E-mail address: haiqing.liu@gmail.com (H. Liu).

0144-8617/$ – see front matter © 2012 Elsevier Ltd. All rights reserved.
http://dx.doi.org/10.1016/j.carbpol.2012.07.033

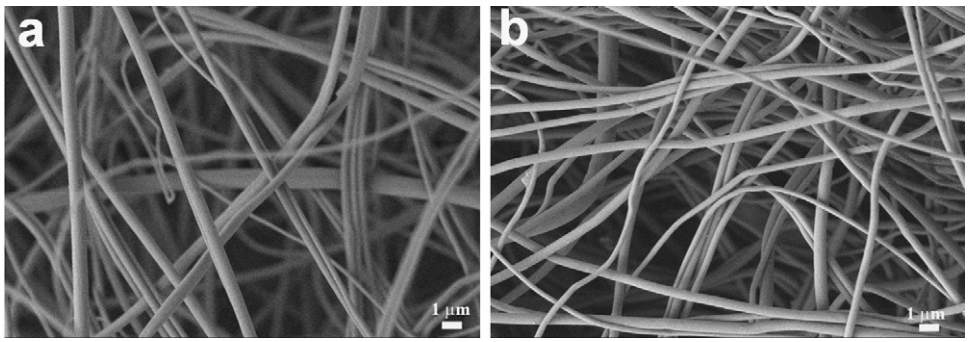

Fig. 1. SEM images of (a) cellulose nanofibers (CelluNF), and (b) phosphorylated cellulose nanofibers (PCelluNF).

(10 nm × 50 nm, thickness × width) and high mechanical properties. Zimmermann et al. (2011) applied negatively charged BC fibers to initiate nucleation of calcium-deficient HAp (cdHAp). They found that the presence of cdHAp crystals on BC fiber surfaces resulted in increased cell attachment. It was reported that phosphorylated BC fibers could effectively induce the growth of carbonate-containing HAp to form a 3D BC/HAp nanocomposite network with appropriate mechanical performance and good osteoconductivity and biodegradation (Wan et al., 2007). These BC/HAp composites can be used for bone healing applications.

It is been known that natural BC fibers do not offer an ability to control the scale of the fibers in the nano- to micro-diameter

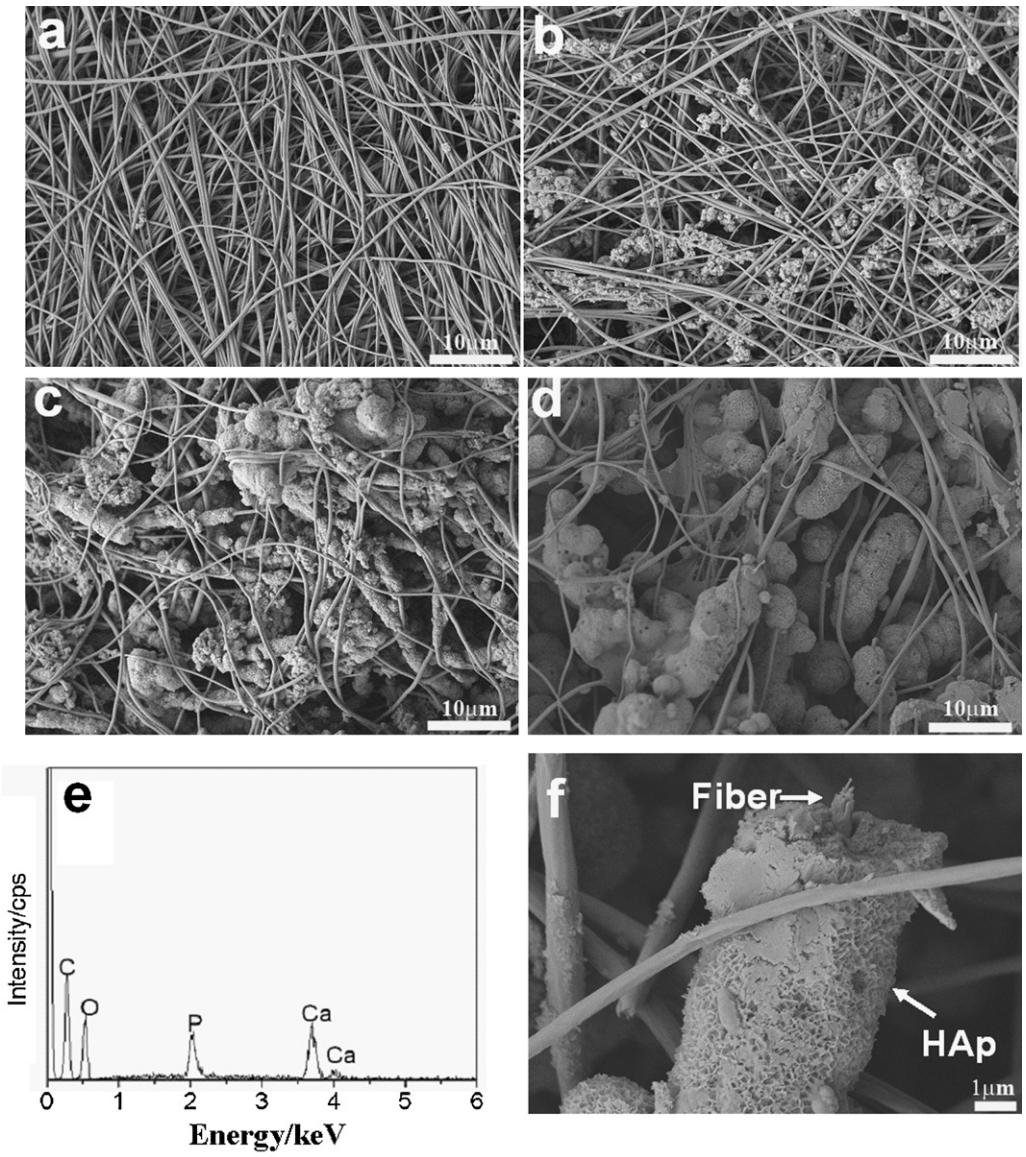

Fig. 2. SEM images of cellulose nanofibers/HAp composites obtained from growth in 1.5SBF for various days. (a) 7d-CelluNF/HAp, (b) 14d-CelluNF/HAp, (c) 21d-CelluNF/HAp, (d) 28d-CelluNF/HAp, EDS spectrum of (e) 7d-CelluNF/HAp and (f) SEM image of a fiber wrapped by HAp.

regions, while the electrospinning technique can produce continuous fibers with controlled diameter (Rodriguez et al., 2011). Electrospun cellulose nanofibers (CelluNF) have been readily obtained from hydrolysis of cellulose acetate nanofibers (Greish, Meetani, Al Matroushi, & Shamsi, 2010; Liu & Hsieh, 2002). Their diameter and alignment can be controlled by adjusting the spinning solution properties and electrospinning parameters (Liao, Wu, Wu, Zhan, & Liu, 2012). So far, electrospun CelluNFs have been used as scaffolds for the growth of HAp in one case only. Renneckar et al. (Rodriguez et al., 2011) reported biomimetic calcium phosphate crystal mineralization on these scaffolds. They exposed CelluNFs to carboxymethyl cellulose (CMC) adsorption, in order to generate carboxyl groups on fiber surfaces. It was found that such a pretreatment may effectively catalyze the calcium phosphate mineralization on the fibers. Because the CMC is physically adsorbed on the fibers, the HAp crystals wrap around the CelluNFs with a pearl-on-string type of arrangement.

In this work, we intended to chemically modify the electrospun CelluNF surfaces by a phosphorylation reaction. The phosphate groups may bond with Ca^{2+} through coordination bonds, and then induce the growth of Ca–P crystals. The morphology, elemental composition and structure of CelluNF/HAp composites were characterized by scanning electron microscopy (SEM), transmission electron microscopy (TEM), Fourier transform infrared spectroscopy (FTIR), X-ray diffraction (XRD) and X-ray photoelectron spectroscopy (XPS). Due to the high HAp induction activity, the phosphorylated electrospun CelluNF is a good alternative to collagen fiber in the biomimetic fabrication of fiber/HAp composites. Such composites may be potentially used as bone tissue engineering materials.

2. Experimental

2.1. Materials

Cellulose acetate (CA) (M_η = 30,000, acetyl content 39.8%) were purchased from Aldrich, USA. Orthophosphoric acid (85%), triethyl phosphate, phosphorous pentoxide and hexanol were bought from Sinopharm Chemical Regent Co. (Shanghai, China). All chemicals were of analytical grade, and were used as received.

2.2. Preparation of CelluNF and phosphorylation treatment

CA nanofibers were first fabricated according to our previous work (Liao et al., 2012). Briefly, a spinning solution of 20 wt% CA in 2:1(v/v) acetone/*N*,*N*-dimethylacetamide (DMAc) was prepared and degassed. It was then filled into a syringe with a stainless needle of gauge 16 (inner diameter 0.8 mm). A positive electrode was clamped on the needle and connected to a power supply (DW-P303-IAC, Tianjin Dongwen High Voltage Plant, Tianjin, China). The grounded counter electrode was connected to cardboard covered with aluminum (Al) foil as a collector. The electrical field was 0.8 kV/cm. The feeding rate was 12 μL/min monitored by a syringe pump (TS2-60, Longer Precision Pump Co. Ltd, Baoding, China). During electrospinning, the environmental temperature and humidity were 27 ± 1 °C and 65 ± 3%, respectively. The CA nanofibers were hydrolyzed in 0.05 mol/L NaOH/ethanol solution for 24 h at room temperature, followed by thoroughly washing with double-distilled (DD) water until the supernatant reached neutral. They were freeze-dried to obtain CelluNFs. The dried CelluNFs were stored in a desiccator until use. Their FTIR spectrum (not shown here) confirmed that the absence of absorption peak at 1753 cm^{-1} for the stretching vibration of carbonyl groups, suggesting that cellulose acetate were converted to cellulose (Rodriguez et al., 2011).

To a mixed solvent of H_3PO_4 (20 mL), ethanol (20 mL), and hexanol (25 mL) in a round bottom flask, 62.5 g of P_2O_5 was added. A homogeneous clear solution was obtained after magnetic stirring for 2 h. 2.0 g of CelluNF, which was sequentially pre-swollen in ethanol and hexanol for respective 24 h, were soaked in the solution. The phosphorylation reaction of CelluNF was proceeded under magnetic stirring for 72 h at 35 °C. Then the phosphorylated CelluNF (PCelluNF) were taken out and thoroughly rinsed with DD water, followed by vacuum-drying at 40 °C for 24 h.

2.3. Biomimetic growth of HAp on PCelluNF

The 1.5 times simulated body fluid (1.5SBF) was prepared as follows. Sodium chloride (15.5801 g), sodium hydrogen carbonate (0.7057 g), potassium chloride (0.7455 g), disodium hydrogen phosphate dodecahydrate (1.0744 g), and magnesium chloride hexahydrate (0.6099 g) were sequentially added and dissolved into 1700 mL of DD water. Its pH value was adjusted to 7.4 by 1 mol/L HCl aqueous solution. Then 0.8325 g of anhydrous calcium chloride and 0.1420 g of sodium sulfate were dissolved into the solution. Its pH value was re-adjusted to 7.40 by tris-hydroxymethyl aminomethane. The final total volume was adjusted to 2000 mL by adding double-distilled water.

The CelluNFs and PCelluNFs were soaked in 1.5SBF solution at 37 °C for 5, 7, 14, 21 and 28 days. Fresh 1.5SBF solution was replaced once per day. The samples were taken out and rinsed with DD water. Finally the CelluNF/HAp composites were freeze-dried. Accordingly, they were coded as for example 5d-CelluNF/HAp, "5d" represents five culturing days.

2.4. Characterization

The diameter and morphology of nanofibers and composites were observed by SEM (JEOL JSM-7500F) and TEM (JEOL JEM-2010). All samples were sputter-coated with platinum before SEM observation. For TEM measurement, composite fibers were dispersed ultrasonically in ethanol and were transferred onto Formvar-coated copper grids before observation. FTIR spectra were collected on thermo-Nicolet 5700 spectrometer in KBr form. The XRD patterns were recorded on X'pert MPD Pro (Philips) with Cu Kα radiation (λ = 1.542 Å), at 2θ angles ranging from 5 to 80°, accelerating voltage of 40 kV, emission current of 30 mA and scanning speed of 8 min^{-1}. XPS was carried out on a PHI 5000 Instrument (ESCA LAB MKII) with an Al Kα anode. All binding energies (B.E.) were referenced to the neutral C_{1s} peaks at 284.8 eV. Surface elemental stoichiometries were determined from the sensitivity-factor-corrected peak-area ratios, and the software XPSpeak 4 was used to fit the XPS spectra peaks. The porosity and specific surface areas were characterized by nitrogen adsorption–desorption isotherm analysis (Micromeritics ASAP2020 apparatus at 77 K). The viscosity molecular weight (M_η) of cellulose nanofibers was determined with cadoxen as the solvent at 25 °C by using viscometery according to $[\eta] = 3.85 \times 10^{-2} M_w^{0.76}$ (mL g^{-1}) (Brown & Wiskston, 1965).

3. Results and discussion

3.1. Morphology of HAp on CelluNFs

Fig. 1a shows SEM images of CelluNFs regenerated from the hydrolysis of electrospun cellulose acetate nanofibers. In our previous work we have demonstrated that this is a much easier method in fabrication of uniform CelluNFs than a direct electrospinning of cellulose solutions in LiCl/*N*,*N*-dimethylacetamide (Kim, Frey, Marquez, & Joo, 2005; Liu & Hsieh, 2002). The CelluNFs are smooth and circular. They are randomly organized into a highly porous mat. After surface phosphorylation, PCelluNFs display a

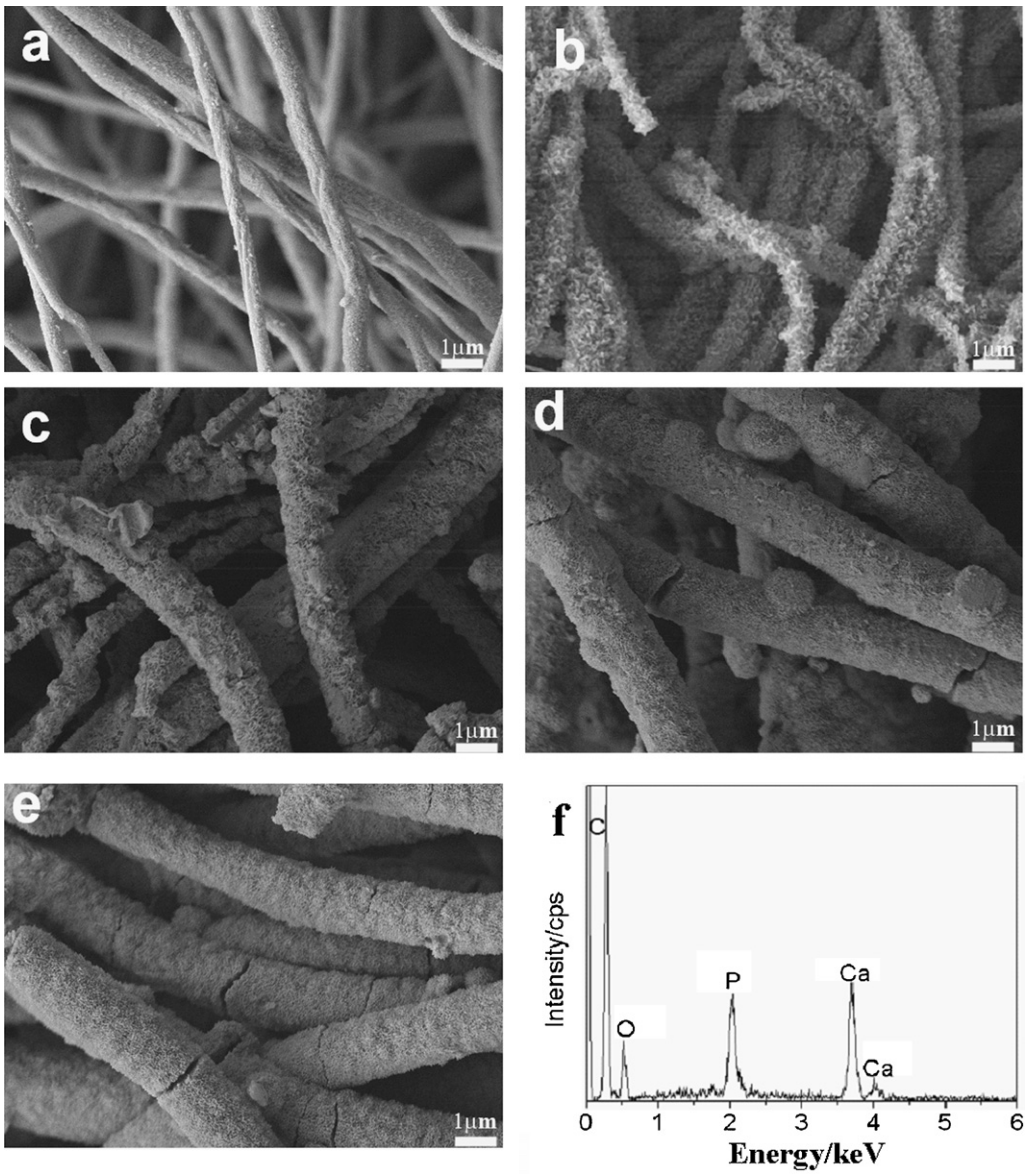

Fig. 3. SEM images of phosphorylated cellulose nanofibers/HAp composites obtained from growth in 1.5SBF for various days. (a) 5d-PCelluNF/HAp, (b) 7d-PCelluNF/HAp, (c) 14d-PCelluNF/HAp, (d) 21d-PCelluNF/HAp, (e) 28d-PCelluNF/HAp and (f) EDS spectrum of 21d-PCelluNF/HAp.

similar smooth surface morphology (Fig. 1b) to that of CelluNFs, suggesting that phosphorylation process does not cause any physical changes to the fibers. The average diameter of both fibers is ~0.56 μm.

Hydroxyl groups are rich on CelluNFs surfaces. They readily react with phosphoric acid to form cellulose phosphate in the mild heterogeneous reaction conditions used in this work. The content of phosphate groups on PCelluNFs was determined to be 1.62 mmol/g by the spectrophotometric method of molybdenum blue (de Magalhaes Padilha, Rocha, Moreira, de Sousa Campos, & do Carmo Federici, 1997). This corresponds to a degree of substitution (phosphate group) of 0.28, indicating that the phosphorylation on CelluNFs is slight. Such a small introduction of phosphate groups onto CelluNFs would not change the main characteristics (like mechanical and solvent-resistivity) of cellulose nanofibers. The viscosity molecular weight of the PCelluNF and CelluNF was 1.51×10^4 and 1.45×10^4, corresponding to a degree of polymerization of 81 and 90, respectively. Thus phosphorylation process indeed caused degradation to the cellulose due to hydrolysis. However, such a nanofibrous mat composed of degraded PCelluNF is still mechanically strong enough as a scaffold material.

The CelluNFs were cultured in 1.5SBF to test the HAp growth on them. Fig. 2 shows the surface morphology of CelluNF/HAp composite fibers. Only a few particles are found on their surfaces on day 7 (Fig. 2a). An energy dispersive X-ray spectroscopy (EDS) spectrum of these particles demonstrates that they contain calcium and phosphorus elements (Fig. 2e). The mole ratio of Ca/P is 1.41, which is less than 1.67 of natural bone (Hutchens, Benson, Evans, O'eill, & Rawn, 2006). More and bigger particles are found on the mat on day 14 (Fig. 2b). The particle size increases further on day 21 and 28 (Fig. 2c and d). Fig. 2c and d display a special morphology, i.e. HAP particles on fiber strings. The particle size and morphology vary greatly, i.e. some grow on CelluNFs, and some use CelluNFs as templates to form cylindrical HAp (Fig. 2f). Such a random HAp growth and non-uniform size and morphology of HAp clusters on CelluNFs are also found on BC fibers (Wan et al., 2007). The reason is that these unmodified cellulose fiber surfaces lack effective functional groups for bonding calcium ions to form nuclei, as will be discussed in the latter section. The EDS spectrum of the HAp clusters on day

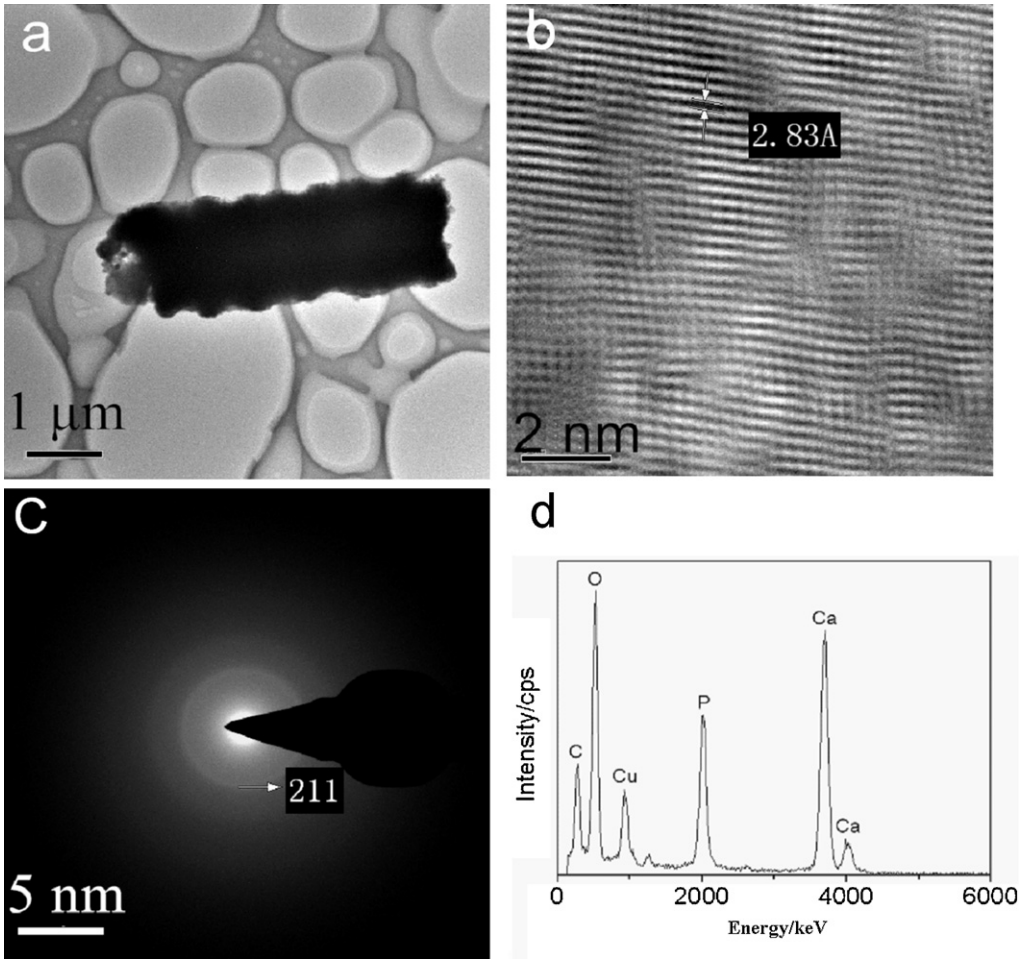

Fig. 4. TEM (a), HR-TEM (b) and SAED (c) image, and EDS spectrum (d) of 14d-PCelluNF/HAp.

28 indicates that they contain calcium and phosphorus elements (not shown here). The Ca/P mole ratio is 1.55, which is still less than that of natural bone, suggesting that the HAp on CelluNFs is calcium deficient, which is independent of culturing time.

The morphologies of HAp on PCelluNFs are displayed in Fig. 3. The fiber surfaces become coarse on day 5 (Fig. 3a). This is due to large amount of tiny HAp particles (<100 nm) grow on the fibers (Fig. 3a). On day 7, all PCelluNFs are completely covered with a layer of flowerlike crystals (Fig. 3b). The average size of PCelluNF/HAp composite fibers increases to 0.67 μm, which is 0.11 μm thicker than that of PCelluNFs (0.56 μm). On day 14 and 21, the HAp crystal layers become thicker and thicker (Fig. 3c and d), the size of composite fibers further increases to 1.79 and 3.19 μm, respectively. Due to fragility of HAp, cracks are observed for the thick HAp layers (Fig. 3d and f). The broken HAp cannot move freely, instead they are restricted by the core fibers, i.e. which act as supporting scaffolds for the HAp. The PCelluNF/HAp composites keep the 3D porous structure as that of the PCelluNF mat. From EDS analysis (Fig. 3f), the Ca/P mole ratio of HAp crystals on PCelluNFs on day 21 is ca. 1.57, indicating that these HAps are still calcium deficient. Compared to the poor growth of HAp on CelluNFs, the HAp grows more easily, quickly and uniformly on PCelluNFs, and each PCelluNF is entirely covered with a HAp crystal layer. The growth of HAp layer on PCelluNFs increases almost linearly with time between 7 and 21 days with a growth constant of ca. 0.18 μm/day. In a similar study, the HAp growth on electrospun cellulose nanofibers could be enhanced by introducing carboxylate groups onto their surfaces through physical adsorption of CMC. A large amount of HAp "blossoms" were formed on cellulose nanofiber surfaces (Rodriguez et al., 2011). In comparison, HAp crystals grow more uniformly on our phosphorylated cellulose nanofibers than on the CMC treated ones.

Fig. 4 shows TEM images of the 14d-PCelluNF/HAp composite. The HAp crystal lattice spacing is 0.283 nm (Fig. 4b), which corresponds to the (2 1 1) crystallographic plane. The brightest diffraction ring in the selected area electron diffraction (SAED) image is designated to the (2 1 1) plane of HAp (Fig. 4c), with a lattice spacing of 0.281 nm. The EDS spectrum shows that the Ca/P mole ratio is ca. 1.48.

3.2. Fiber surface chemical structure

The different HAp growth behavior on CelluNF and PCelluNF must be related to their surface chemical structure. XPS is a very effective tool in characterizing the chemical structure and elemental composition on fiber surfaces. Compared to CelluNFs, the survey scan XPS spectrum of PCelluNF (Fig. 5A) shows a new peak at 133.02 eV of P_{2p} (Cai, Zhang, Zeng, & Sun, 2011). This suggests that phosphate groups were introduced onto PCelluNFs. For PCelluNF/HAp composite fibers, new peaks at 132.93 and 346.97 eV for P_{2p} of P^{5+} and Ca_{2p} of Ca^{2+}, respectively, are displayed in its XPS spectrum (Fig. 5A–C). Therefore, the crystals formed on PCelluNFs contain P and Ca elements.

The high resolution scan XPS spectra of C_{1s} are shown in Fig. 5B. They are deconvoluted into three sub-peaks by curve fitting. These three sub-peaks correspond to three types of carbon-oxygen bonds. The CelluNF displays peaks at 284.4 (shoulder), 285.9 (strong), and 287.2 (shoulder) eV for —C*—C—, —C*—O— and —O—C*—O— (in

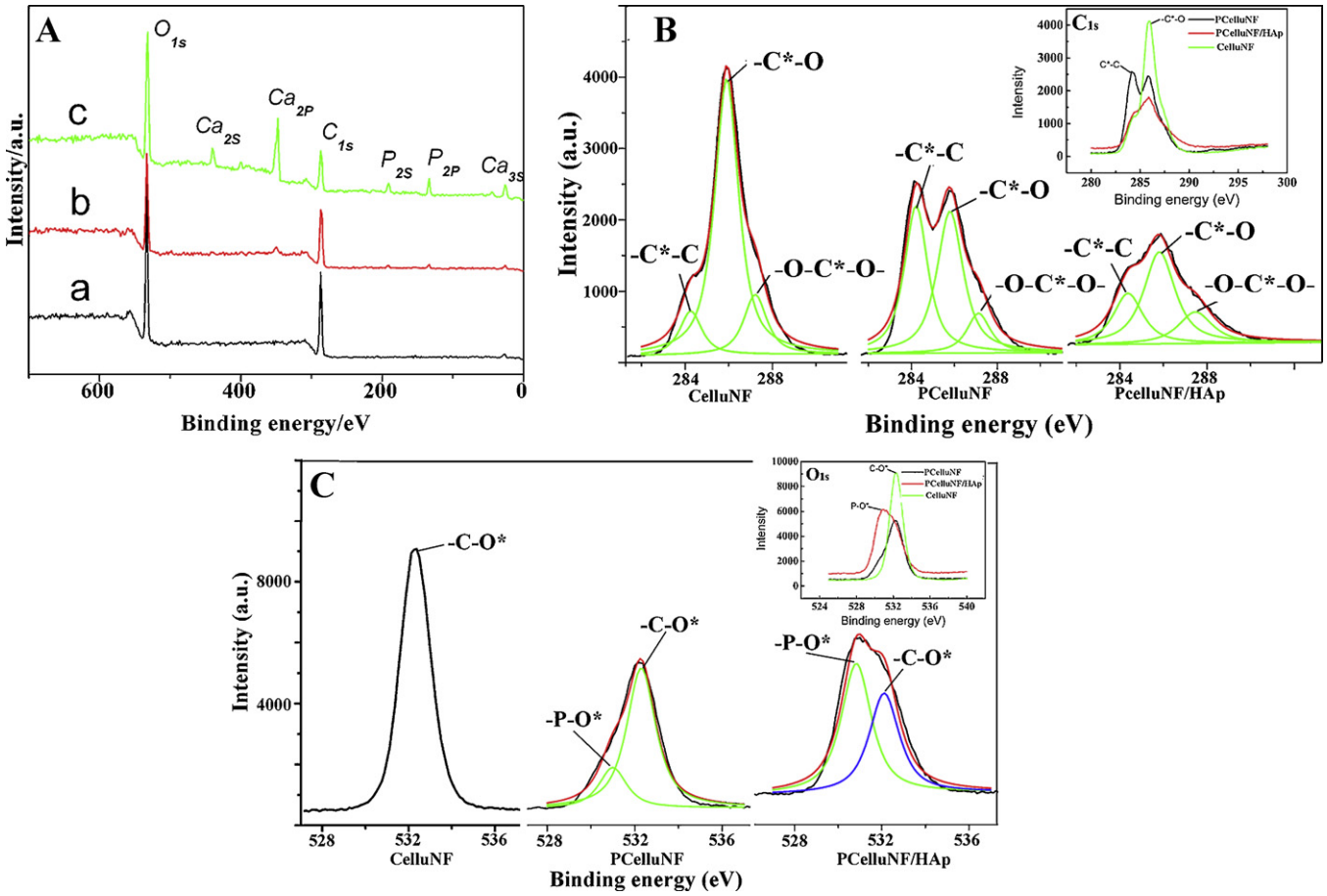

Fig. 5. (A) XPS survey spectra of CelluNF (a), PCelluNF (b), 14d-PCelluNF/HAp (c). High resolution scan of C_{1s} (B) and O_{1s} (C).

the anhydroglucose unit rings) (Xu, Zhao, Kang, Neoh, & Li, 2007), respectively. The corresponding relative carbon content is 10.88%, 73.68% and 15.44% for —C*—C—, —C*—O— and —O—C*—O—, respectively. For PCelluNFs, the positions of the three sub-peaks of C_{1s} are almost same to those of CelluNF (Fig. 5B inset). However, the peak intensity of —C*—C— increases, whereas that of —C*—O— decreases. The substitution of hydroxyl hydrogens with phosphate groups changes the chemical environment of carbon atoms, resulting in a reduction of peak intensity of —C*—O—, and an increasing of that of —C*—C—. For the PCelluNF/HAp composite, the curve fitting gives three sub-peaks at 284.4, 285.5, and 287.5 eV for —C*—C, —C*—O— and —O—C*—O—, respectively. Compared to CelluNF and PCelluNF, the overall intensity of C_{1s} of PCelluNF/HAp greatly decreases. This is because the outer surface of PCelluNF/HAp composite is composed of a thick layer of HAp, as shown in the SEM images.

A symmetrical and strong O_{1s} peak at 532.28 eV for —C—O*— is shown in the high resolution scan XPS spectrum of CelluNF (Fig. 5C). After phosphorylation, the spectrum changes to asymmetrical for PCelluNF. The main O_{1s} peak still locates at 532.28 eV for —C—O*—, but a weak shoulder peak appears at 530.82 eV for —P—O*— (Cai et al., 2011). The oxygen composition in the form of —P—O*— accounts for 21.64% in the total oxygen (—C—O*— plus —P—O*—), corresponding to a degree of substitution (DS) of phosphate groups in the PCelluNF of ca. 0.275, which is close to the value (0.28) obtained from the spectrophotometric method. For PCelluNF/HAp composites, the asymmetrical peak is obviously different from that of PCelluNF. The peak is deconvoluted into two subpeaks respectively located at 530.80 eV (—P—O*—) of the phosphate groups, 532.10 eV (—C—O*—) of carbonate groups (Dahle, Voigts, & Maus-Friedrichs, 2012).

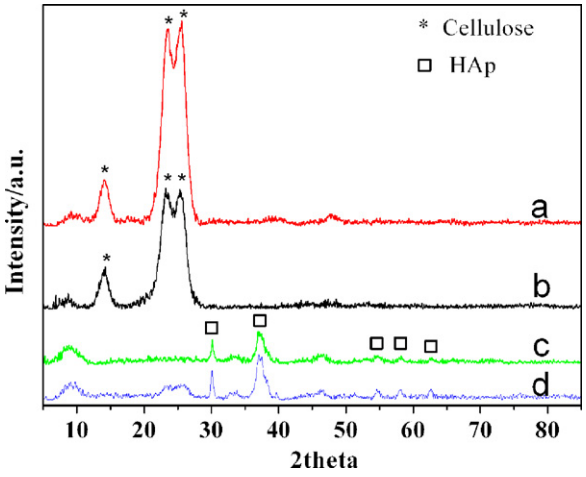

Fig. 6. XRD patterns of (a) CelluNF, (b) PCelluNF, (c) 14d-CelluNF/HAp and (d) 14d-PCelluNF/HAp.

3.3. XRD analysis

The XRD pattern of CelluNFs shows characteristic peaks at 2θ of 12.1, 21.5, and 23.5° for the crystallographic planes (1 0 1), (1 1 0) and (0 0 2) of cellulose II diffraction (Isogai, Usuda, Kato, Uryu, & Atalla, 1989) (Fig. 6), respectively. The sharp peak shape indicates that the crystallinity of CelluNFs is high (Fig. 6a), similar to the result reported by Gatenholm and coworkers (Rodriguez et al., 2011). This

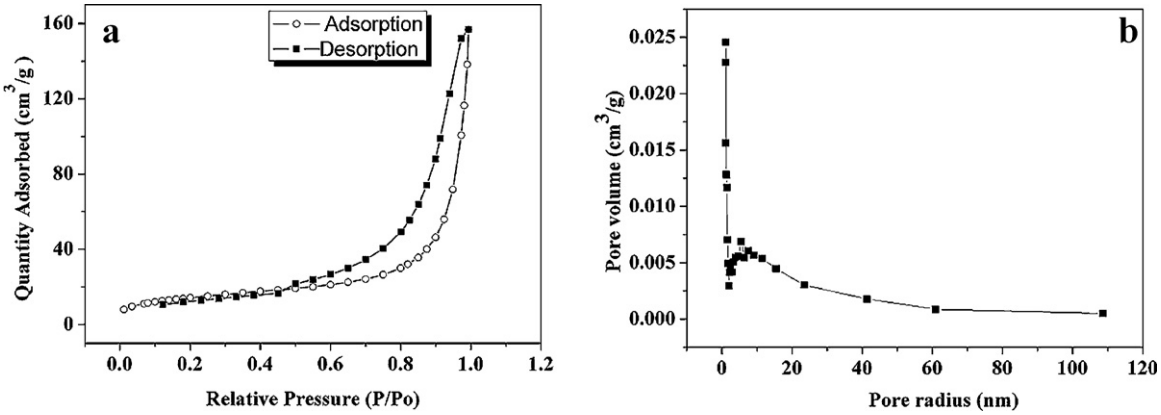

Fig. 7. (a) Nitrogen absorption–desorption isotherms and (b) pore size distribution of 14d-PCelluNF/HAp.

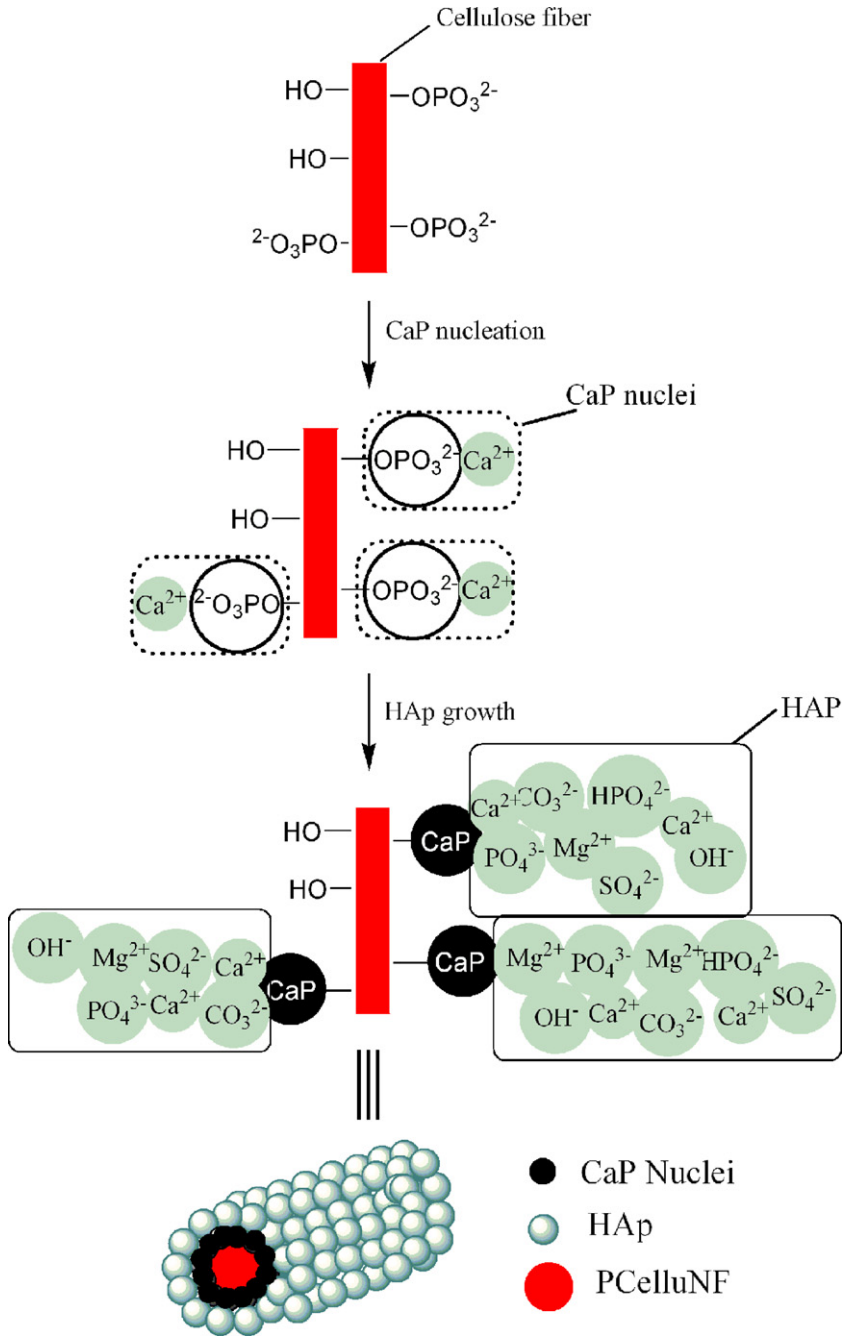

Fig. 8. (A) Surface modification of cellulose nanofibers by phosphorylation reaction to make PCelluNF and (B) formation of HAp layer on PCelluNF.

is due to that the CelluNFs were regenerated from cellulose acetate nanofibers in aqueous solutions. The pattern of PCelluNF is similar to that of CelluNF (Fig. 6b), suggesting that the phosphorylation process did not destroy the crystal structure of CelluNFs. The patterns of CelluNF/HAp and PCelluNF/HAp (Fig. 6c and d) present characteristic peaks at 26.2, 32.6° for (0 0 2) and (1 1 2) crystallographic planes of HAp (He et al., 2012), respectively, confirming that the crystals on the CelluNF and PCelluNFs are HAp. Because the CelluNFs are covered by a thick layer of HAp crystals, the characteristic peaks of cellulose are not observed on the XRD patterns of CelluNF/HAp and PCelluNF/HAp. The peak intensities of PCelluNF/HAp (Fig. 6d) are stronger and sharper than that of CelluNF/HAp (Fig. 6c), indicating that the crystallinity and crystal size of HAp on PCelluNF/HAp is larger than that on CelluNF/HAp. According to the "Scherrer equation", the average crystallite size of HAp in the (0 0 2) plane is calculated to be 20 and 24 nm for CelluNF/HAp and PCelluNF/HAp, respectively. The difference in crystallite size of the HAp on these two kinds of cellulose nanofibers should be related to the mechanisms of the nucleus formation, as will be discussed in the latter section of nucleation and growth mechanism.

3.4. Pore structure

Fig. 7a shows the N_2 adsorption–desorption isotherms of the 14d-PCelluNF/HAp composite. They belong to type IV isotherms with type H_3 hysteresis when the relative pressure P/P_o is in a range of 0.6–1.0 according to the IUPAC nomenclature. In a narrow relative pressure P/P_o of 0.80–0.95, the N_2 adsorption sharply increases. This is a characteristic process of adsorption into the mesopores (Liu, Huang, Xiao, & Liu, 2010). In the relative pressure P/P_o of 0–0.5, the N_2 adsorption increased slowly with the pressure, then almost steadied till P/P_o of 0.5, suggesting that the existence of micropores in the composites. Fig. 7b shows the corresponding pore size distribution (PSD) curve, which was derived by the Barret–Joyner–Halenda (BJH) method. It reveals a pore size distribution of mesopores in a range of 2–18 nm, and large amount of micropores in a range of 1.03–2.0 nm. These micro- and meso-pores distribute in the HAp particles. Additionally, among the PCelluNF/HAp fibers the mats naturally form large amount of interconnected macropores of several to tens of micrometer in diameter, as shown in their SEM images (Fig. 3). These PCelluNF/HAp composite fibrous mats are promising scaffolds due to their hierarchical porosity including macro-, meso-, and micro-pores (García, Izquierdo-Barba, Colilla, de Laorden, & Vallet-Regí, 2011). These different scale pores are beneficial to the adhesion, proliferation and migration of cells, and to the mass (nutrients and metabolites) transportation through the scaffolds. The Brunauer–Emmett–Teller (BET) analysis showed that the specific surface areas of the composite are 51.08 m^2/g.

3.5. Mechanism of nucleation and HAp growth

The formation of HAp crystals on CelluNFs involves two sequent processes, i.e. nucleation and growth. This nucleation is referred to the calcium immobilization. Due to different efficiencies in the capturing of calcium ion, the functional groups on fiber surfaces play key roles in the nucleation. The hydroxyl groups on CelluNFs interact with calcium ions through ion-dipolar forces. It is very weak, resulting in low efficient nucleation by the trapping of calcium ions, and therefore the HAp growth on CelluNFs is very poor (Fig. 2). Therefore, though CelluNF possesses abundant hydroxyl groups, they are not effective binding groups for calcium ions. However, little amount of carboxylate groups would be introduced onto the CelluNFs because of occurrence of cellulose scission and aerobic oxidation in the alkaline hydrolysis process (Knill & Kennedy, 2003; Rodriguez et al., 2011). These negatively charged carboxylate groups can bind the positively charged calcium ions through coordination bonds to form calcium carbonates, which then act as nuclei inducing the growth of HAp, but only a small amount of HAp crystals formed and wrapped a few CelluNFs at day 14 (Fig. 2b). Therefore, in SBF, CelluNFs only show slight HAp induction activity, similar to other cellulose materials (Märtson et al., 1999). A weak activity in forming of HAp crystals was observed for unmodified BC fibers (Wan et al., 2007).

Phosphorylation of CelluNFs changes their surface chemistry (Fig. 8A). As indicated by the XPS spectrum, phosphate groups were detected on PCelluNFs surfaces (Fig. 5A). Through ionic interactions, phosphate groups can easily capture calcium ions in SBF to form calcium phosphate (Ca–P) nuclei, and induce the growth of HAp crystals. As shown in the SEM images of PCelluNF/HAp composites, HAp crystals grow into cylindrical layers on each PCelluNF, suggesting that the PCelluNFs are highly bioactive. A schematic diagram of the PCelluNF/HAp composite is shown in Fig. 8B.

4. Conclusions

Electrospun CelluNFs and their slightly phosphorylated products were evaluated as templates to induce biomimetic growth of HAp crystals. We found that the unmodified CelluNFs showed very low bioactivity toward the HAp growth, whereas the slightly phosphorylated CelluNFs were highly active with an ability to interact with Ca^{2+} ions to form Ca-P nuclei. HAp crystals in uniform size and morphology were grown on the modified CelluNFs. The as-obtained HAp is calcium deficient with part of the phosphate groups substituted with carbonate and phosphite groups. The CelluNF/HAp composites had mesopores in a range of 2–18 nm, and large amount of micropores in a range of 1.03–2.0 nm, in addition to many pores in the micrometer range formed among fibers. The specific surface areas of the composite were 51.08 m^2/g. The high HAp induction bioactivity of the phosphorylated electrospun CelluNFs makes them applicable in the biomimetic fabrication of fiber/HAp composites. Such composites may be promising bone tissue engineering materials.

Acknowledgements

This work is supported by the Natural Science Foundation of Fujian Province (2010J06017), the National Basic Research Program of China (2010CB732203), and the National Natural Science Foundation of China (No. 50973019).

References

Backdahl, H., Helenius, G., Bodin, A., Nannmark, U., Johansson, B. R., Risberg, B., et al. (2006). Mechanical properties of bacterial cellulose and interactions with smooth muscle cells. *Biomaterials*, *27*(9), 2141–2149.

Brown, W., & Wiskston, R. (1965). A viscosity–molecular weight relationship for cellulose in cadoxen and hydrodynamic interpretation. *European Polymer Journal*, *1*, 1–10.

Cai, Y. L., Zhang, S., Zeng, X. T., & Sun, D. (2011). Effect of fluorine incorporation on long-term stability of magnesium-containing hydroxyapatite coatings. *Journal of Materials Science: Materials in Medicine*, *22*(7), 1633–1638.

Collins, A. M., Skaer, N. J. V., Gheysens, T., Knight, D., Bertram, C., Roach, H. I., et al. (2009). Bone-like resorbable silk-based scaffolds for load-bearing osteoregenerative applications. *Advanced Materials*, *21*(1), 75–78.

Dahle, S., Voigts, F., & Maus-Friedrichs, W. (2012). In situ preparation of calcium carbonate films. *Thin Solid Films*, *520*(6), 1842–1846.

de Magalhaes Padilha, P., Rocha, J. C., Moreira, J. C., de Sousa Campos, J. T., & do Carmo Federici, C. (1997). Preconcentration of heavy metals ions from aqueous solutions by means of cellulose phosphate: An application in water analysis. *Talanta*, *45*(2), 317–323.

Entcheva, E., Bien, H., Yin, L., Chung, C.-Y., Farrell, M., & Kostov, Y. (2004). Functional cardiac cell constructs on cellulose-based scaffolding. *Biomaterials*, *25*(26), 5753–5762.

García, A., Izquierdo-Barba, I., Colilla, M., de Laorden, C. L., & Vallet-Regí, M. (2011). Preparation of 3-D scaffolds in the SiO_2–P_2O_5 system with tailored hierarchical meso-macroporosity. *Acta Biomaterialia*, *7*(3), 1265–1273.

Greish, Y. E., Meetani, M. A., Al Matroushi, E. A., & Shamsi, B. A. (2010). Effects of thermal and chemical treatments on the structural stability of cellulose acetate nanofibers. *Carbohydrate Polymers*, *82*(3), 569–577.

Hartgerink, J. D., Beniash, E., & Stupp, S. I. (2001). Self-assembly and minerization of peptide-amphiphile nanofibers. *Science*, *294*, 1684–1688.

He, M., Chang, C., Peng, N., & Zhang, L. (2012). Structure and properties of hydroxyapatite/cellulose nanocomposite films. *Carbohydrate Polymers*, *87*(4), 2512–2518.

Hutchens, S. A., Benson, R. S., Evans, B. R., O'eill, H. M., & Rawn, C. J. (2006). Biomimetic synthesis of calcium-deficient hydroxyapatite in a natural hydrogel. *Biomaterials*, *27*(26), 4661–4670.

Isogai, A., Usuda, M., Kato, T., Uryu, T., & Atalla, R. H. (1989). Solid-state CP/MAS carbon-13 NMR study of cellulose polymorphs. *Macromolecules*, *22*(7), 3168–3172.

Juhasz, J. A., & Best, S. M. (2012). Bioactive ceramics: Processing, structures and properties. *Journal of Materials Science*, *47*(2), 610–624.

Kim, C. W., Frey, M. W., Marquez, M., & Joo, Y. L. (2005). Preparation of submicron-scale, electrospun cellulose fibers via direct dissolution. *Journal of Polymer Science Part B: Polymer Physics*, *43*(13), 1673–1683.

Klemm, D., Schumann, D., Udhardt, U., & Marsch, S. (2001). Bacterial synthesized cellulose-artificial blood vessels for microsurgery. *Progress in Polymer Science*, *26*(9), 1561–1603.

Knill, C. J., & Kennedy, J. F. (2003). Degradation of cellulose under alkaline conditions. *Carbohydrate Polymers*, *51*, 281–300.

Liao, H. Q., Wu, Y. Q., Wu, M. Y., Zhan, X. R., & Liu, H. Q. (2012). Aligned electrospun cellulose fibers reinforced epoxy resin composite films with high visible light transmittance. *Cellulose*, *19*(1), 111–119.

Liu, H. Q., & Hsieh, Y. L. (2002). Ultrafine fibrous cellulose membranes from electrospinning of cellulose acetate. *Journal of Polymer Science Part B: Polymer Physics*, *40*(18), 2119–2129.

Liu, R. L., Huang, Y. X., Xiao, A. H., & Liu, H. Q. (2010). Preparation and photocatalytic property of mesoporous ZnO/SnO_2 composite nanofibers. *Journal of Alloys and Compounds*, *503*(1), 103–110.

Märtson, M., Viljanto, J., Hurme, T., Laippala, P., & Saukko, P. (1999). Is cellulose sponge degradable or stable as implantation material? An in vivo subcutaneous study in the rat. *Biomaterials*, *20*(21), 1989–1995.

Miyamoto, T., Takahashi, S., Ito, H., Inagaki, H., & Noishiki, Y. (1989). Tissue biocompatibility of cellulose and its derivatives. *Journal of Biomedical Materials Research*, *23*, 125–133.

Rodriguez, K., Renneckar, S., & Gatenholm, P. (2011). Biomimetic calcium phosphate crystal mineralization on electrospun cellulose-based scaffolds. *ACS Applied Materials and Interfaces*, *3*(3), 681–689.

Wan, Y. Z., Gao, C., Luo, H. L., He, F., Liang, H., Li, X. L., et al. (2009). Early growth of nano-sized calcium phosphate on phosphorylated bacterial cellulose nanofibers. *Journal of Nanoscience and Nanotechnology*, *9*(11), 6494–6500.

Wan, Y. Z., Huang, Y., Yuan, C. D., Raman, S., Zhu, Y., Jiang, H. J., et al. (2007). Biomimetic synthesis of hydroxyapatite/bacterials cellulose nanocomposites for biomedical applications. *Materials Science and Engineering C: Biomimetic and Supramolecular Systems*, *27*, 855–864.

Xu, F. J., Zhao, J. P., Kang, E. T., Neoh, K. G., & Li, J. (2007). Functionalization of nylon membranes via surface-initiated atom transfer radial polymerization. *Langmuir*, *23*, 8585–8592.

Zimmermann, K. A., LeBlanc, J. M., Sheets, K. T., Fox, R. W., & Gatenholm, P. (2011). Biomimetic design of a bacterial cellulose/hydroxyapatite nanocomposite for bone healing applications. *Materials Science and Engineering C: Materials for Biological Applications*, *31*(1), 43–49.